Virtual Reality Based Shading Pattern Recognition and Interactive Global Maximum Power Point Tracking in Photovoltaic Systems

Kangshi Wang, *Member*, *IEEE*, Jieming Ma, *Senior Member*, *IEEE*, Xiao Lu, Jingyi Wang, Ka Lok Man, Kaizhu Huang, *Member*, *IEEE*, and Xiaowei Huang, *Member*, *IEEE*

***Abstract*—The performance of photovoltaic (PV) systems is influenced by various factors, including atmospheric conditions, geographical locations, and spatial and temporal characteristics. Consequently, the optimization of PV systems relies heavily on the global maximum power point tracking (GMPPT) methods. In this paper, we adopt virtual reality (VR) technology to visualize PV entities and simulate their performances. The integration of VR technology introduces a novel spatial and temporal dimension to the shading pattern recognition (SPR) of PV systems, thereby enhancing their descriptive capabilities. Furthermore, we introduce an interactive GMPPT (IGMPPT) method based on VR technology. This method leverages interactive search techniques to narrow down search regions, thereby enhancing the search efficiency. Experimental results demonstrate the effectiveness of the proposed IGMPPT in representing the spatial and temporal characteristics of PV systems and improving the efficiency of GMPPT.**

***Index Terms*—Photovoltaic (PV) system, virtual reality (VR), shading pattern recognition (SPR), global maximum power point tracking (GMPPT).**

I. Introduction

PHOTOVOLTAIC (PV) systems have gained popularity as a sustainable way to harness solar energy, owing to their eco-friendliness, low operating costs, and silent operation [1]. However, the performance of PV systems can be impacted by partial shading conditions (PSCs) arising from neighbouring objects such as buildings, trees, and clouds [2]. PSCs create a discrepancy in the current between shaded and unshaded PV modules (PVMs), resulting in multiple peaks in the output power-voltage (*P-V*) curve. To accurately detect the shading patterns and identify the global maximum power point (GMPP), an efficient and accurate GMPP tracking (GMPPT) method is crucial for PV systems.

The conventional GMPPT methods can be categorized into two groups: online and offline GMPPT methods [3]. Online GMPPT methods produce real-time control signals based on instantaneous measurements of voltage and current outputs from PV systems. In contrast, offline GMPPT methods employ the model of PV system to formulate the control algorithm.

The perturbation and observation (P&O) method is one of the most widely employed online GMPPT methods [4]. It employs a tracking strategy centred around perturbation-based active sensing. Although its implementation is uncomplicated, the effectiveness is confined to tracing the GMPP solely under the uniform irradiance conditions (UICs). Its accuracy and efficiency are sub-optimal when it is used to deal with PSCs. Therefore, numerous online bio-inspired optimization methods, including logarithmic particle swarm optimization (LPSO) [5], deterministic particle swarm optimization (DPSO) [6], flashing fireflies [7], etc., have been proposed. However, these bio-inspired optimization methods come with certain limitations, such as relying on a single sampling approach, being dependent on specific parameter configurations, and experiencing confusion when dealing with similar maximum power points (MPPs). These limitations occasionally result in an inability to accurately pinpoint the GMPP. The problem associated with the online GMPPT methods lies in their incapacity to swiftly adjust to various atmospheric conditions. They lack the capability to formulate decisions grounded in real-time alterations under the atmospheric conditions and are devoid of empirical expertise.

Conversely, the offline GMPPT methods rely on empirical expertise. An example of offline GMPPT methods is the fractional open-circuit voltage method and the fractional short-circuit current method [8]. These methods leverage predetermined ratios involving the voltage at the GMPP and the open-circuit voltage, or the current at the GMPP and the short-circuit current. These ratios serve as guiding principles for the GMPPT process. Furthermore, [9] proposes an im-

Manuscript received: November 9, 2023; revised: February 23, 2024; accepted: April 28, 2024. Date of CrossCheck: April 28, 2024. Date of online publication: May 29, 2024.

This research was supported by the Suzhou Science and Technology Project-Key Industrial Technology Innovation (No. SYG202122), the XJTLU Postgraduate Research Scholarship (No. PGRS1906004), and the XJTLU AI University Research Centre and Jiangsu (Provincial) Data Science and Cognitive Computational Engineering Research Centre.

K. Wang, J. Ma (corresponding author), X. Lu, J. Wang, and K. L. Man are with the School of Advanced Technology, Xi'an Jiaotong-Liverpool University, Suzhou 215123, China (e-mail: kangshi.wang19@student.xjtlu.edu.cn; jieming.ma@xjtlu.edu.cn; xiao.lu21@student.xjtlu.edu.cn; jingyi.wang1903@student.xjtlu.edu.cn; Ka.Man@xjtlu.edu.cn).

K. Huang is with the Data Science Research Center, Duke Kunshan University, Suzhou 215316, China (e-mail: kaizhu.huang@dukekunshan.edu.cn).

X. Huang is with the School of Computer Science, the University of Liverpool, Liverpool, U.K. (e-mail: xiaowei.huang@liverpool.ac.uk).

DOI: 10.35833/MPCE.2023.000869

proved GMPPT methods for PV systems based on an enhanced offline $0.8V_{OC}$-model [10]. Some GMPPT methods based on the analytical models have also been proposed [11]-[13]. However, the accuracy of these GMPPT methods heavily hinges on the precision of the pre-established model. In conclusion, the incorporation of the model introduces empirical data, enabling enhancements in the performance of the GMPPT process. Nonetheless, within the offline GMPPT method, the reliance is placed solely on a rigid model. Consequently, the precision of the offline GMPPT methods falls short and lacks the adaptability required for real-time adjustments.

There are now a range of hybrid methods based on a combination of online tracking and offline models. Reference [14] integrates the online P&O algorithm to explore predefined zones derived from an offline model of PV system. Reference [15] proposes a modified initialization method that uses the offline model of PV system to generate an initial population across the *P-V* curve for the GMPPT. Reference [16] presents a hybrid GMPPT method for PVMs based on a double-diode model. Reference [17] proposes a self-tuning GMPPT method based on the reinforcement learning and Beta (RL-Beta) parameters to improve the performance of GMPPT method in terms of accuracy and speed. However, the reinforcement learning can indeed be time-consuming. Reference [18] proposes an optimized fuzzy logic controller for MPPT of grid-connected PV systems. The optimized fuzzy logic controller leverages a combination of bio-inspired optimization techniques to achieve the GMPP. These methods are not only grounded in empirical guidance but also possess the capacity to dynamically steer tracking in real time. The performance of these methods is improved by incorporating empirical insights. However, the integration of further information remains imperative. Moreover, the current models of PV system still rely heavily on statistical foundations and mathematical frameworks, potentially leading to limitations in shading pattern recognition (SPR) while overlooking the influences of spatial and temporal characteristics.

In recent years, the virtual reality (VR) technology has risen as a promising tool for precisely representing the spatial and temporal characteristics of real-world entities due to its interactivity [19]. VR enables users to interactively engage with simulated 3D environments that closely resemble real-world entities, such as buildings, cities, and landscapes, in a natural and intuitive manner. In the VR system designed in [20], the user is able to engage interactively within the virtual scene, experiencing the PV system as though it were physically installed. Reference [21] presents a VR study of surrounding obstacles in building integrated PV systems for the estimation of the long-term performance of partially shaded PV strings (PVSs). Reference [22] presents the VR model of PV system for trainees or any people who are interested in the solar energy system. This paper presents a novel method for representing the spatial and temporal characteristics of the PV system through the application of VR. This VR-based method has the capacity to surpass the accuracy of conventional models and achieve advanced SPR and power simulation for PV systems interactively. Furthermore, this interactive method enables the extraction of GMPP information, enhancing the operational accuracy and efficiency of PV systems.

The primary contributions of this paper can be summarized as follows.

1) The spatial and temporal characteristics of PV system are described through the application of VR.

2) The VR technology interactively utilizes real-world measurements and VR models to facilitate SPR and power simulation.

3) The VR-based interactive GMPPT (IGMPPT) method is proposed, which uses interactive search to reduce search regions and thereby enhance the search efficiency.

The remainder of this paper is structured as follows. Section II outlines the methodology. In Section III, the experimental results are discussed. Finally, Section IV presents the conclusions.

II. Methodology

As shown in Fig. 1(a), the initial step (*Step 1*) involves constructing a spatial and temporal model of both the PVS and nearby buildings in the VR environment. Figure 1(b) shows the captured PVM images and statistical analysis results of pixel grayscale. Subsequently, the schematic process involves SPR and power simulation, as shown in Fig. 1(c).

A. VR-based PV System Description

The cross-platform VR engine, Unity, serves as a powerful tool for simulating the sun routine and capturing approximate irradiance data on virtual PV panels. This process entails several steps aimed at creating a realistic representation. To begin, a scene is meticulously crafted in Unity to mirror the physical installation of PV panels, including their precise geographic location. In this step, a proportional replication of PV panel configurations and their surrounding environment from the real world is achieved. In this virtual environment, a directional light object is strategically placed to represent the solar position. A script in Unity is crafted to animate the movement of this directional light, meticulously simulating the sun routine across the sky over a day. To achieve a high degree of precision, the solar position algorithm (SPA) is incorporated into the process. Recognized for its accuracy, the SPA is a creation of the National Renewable Energy Laboratory (NREL), designed to compute the solar position with pinpoint precision by considering the date, time, and geographical coordinates. SPA accounts for the factors such as the elliptical orbit, axial tilt, and atmospheric refraction of the earth. Furthermore, the PV panels, along with their nearby buildings and surrounding structures, are meticulously created as the objects within the Unity. A dedicated script is then implemented to capture irradiance data at each point on the PV panel plane, effectively storing this information for further analysis and visualization. The entire process can be conducted offline. The time resolution can be set by the script and determine the frequency at which the GMPPT is initiated.

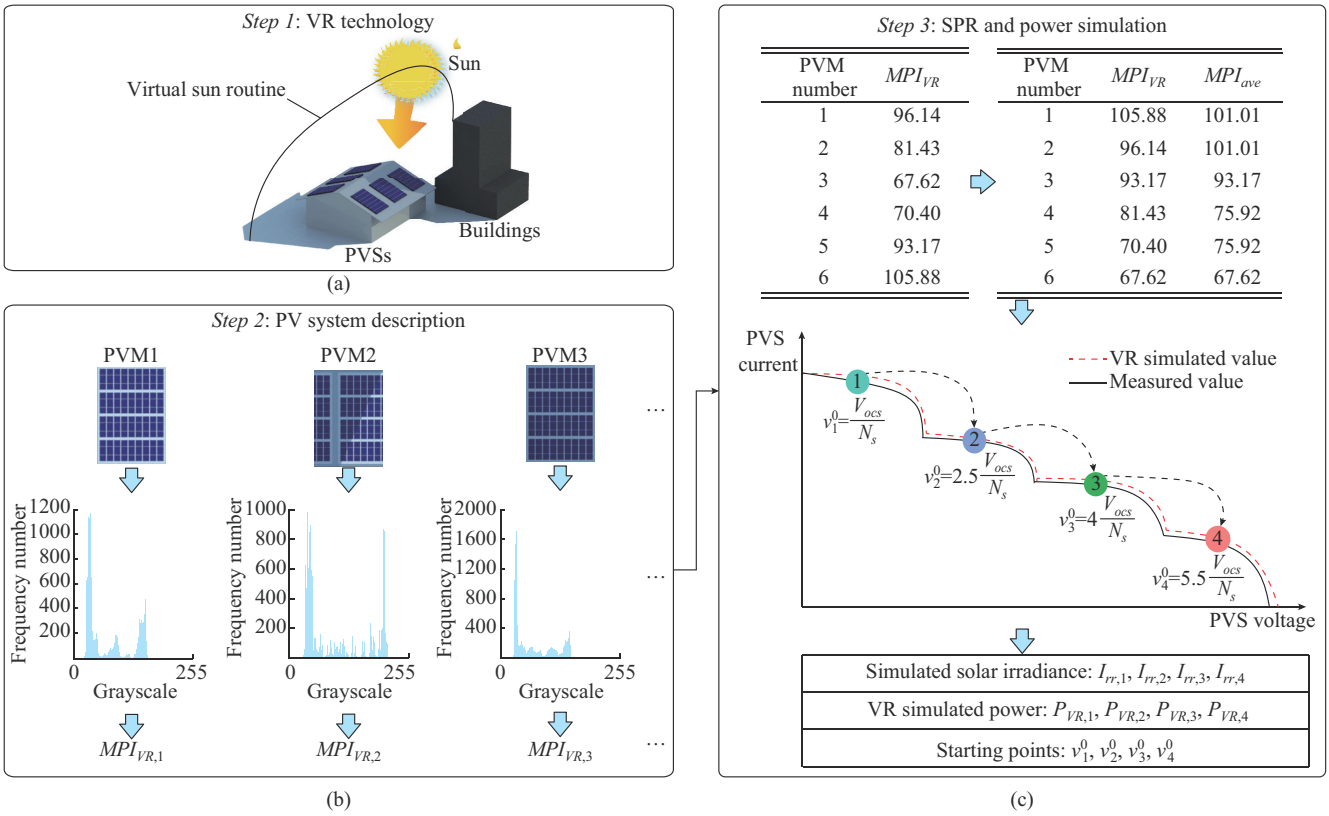

Fig. 1. Schematic illustration of VR-based PV system. (a) Spatial and temporal model of both PVs and nearby building. (b) PVM images and statistical analysis results of pixel grayscale. (c) SPR and power simulation.

The pseudocode presented in Algorithm 1 outlines the procedure for describing the PV system in a VR environment. The PVM images recorded by Unity script are denoted as *Image*. To achieve grayscale conversion of PVM images, Algorithm 1 calculates the mean RGB value of individual pixels and assigns this value to all three colour channels. This process is implemented through the function *im2gray*(·). Subsequently, the algorithm assesses the average brightness of each image, enabling the evaluation of solar irradiance variation across the captures obtained from PVMs. The mean pixel intensity (MPI) of image, denoted as MPI_{VR}, is representative of the average brightness of a capture. A higher MPI_{VR} that signifies the greater solar irradiance is absorbed by the PVM in the VR. An example of the statistical grayscale results for the PVS is depicted in Fig. 1(c), where the MPI_{VR} list is $\{96.17, 81.43, 67.62, 70.40, 93.17, 105.88\}$. Then, the MPI_{VR} list is sorted in descending order and the final result for the MPI_{VR} is $\{105.88, 96.17, 93.17, 81.43, 70.40, 67.62\}$.

To mitigate the modelling complexity in the VR environment to enhance the computational efficiency and model performance, we introduce the concept of MPI tolerance MPI_{tol}. The MPI_{VR} values falling within the range related to MPI_{tol} are averaged. For instance, if MPI_{tol} is set to be 10, the resultant average MPI MPI_{ave} is $\{101.01, 101.01, 93.17, 75.92, 75.92, 67.62\}$. The variable N_{MPI} is used to record the number of PVMs corresponding to each MPI_{VR}, thereby quantifying the number of PVMs that share the same MPI_{ave}. In the scenario shown in Fig. 1(c), N_{MPI} is $\{2, 1, 2, 1\}$. This length of N_{MPI} is denoted as N_{Irr}, serving to count the solar irradiance levels. In this scenario, N_{Irr} equals 4, indicating the existence of four distinct solar irradiance levels associated with this particular PVS.

Algorithm 1: VR-based PV system description

Input: *Image*, number of images N_{IMG}, and MPI tolerance MPI_{tol}
Output: average MPI MPI_{ave}
1: for $i=0$ to N_{IMG}
2: $Grayscale_i=im2gray(Image_i)$
3: end for
4: for $i=0$ to N_{IMG}
5: $MPI_{VR,i}$ equals the average brightness of $Grayscale_i$
6: end for
7: $MPI_{VR}=sort(MPI_{VR},$"*descend*")
8: for $i=0$ to N_{IMG}
9: $SUM=0$
10: for $j=i$ to N_{IMG}
11: if abs$(MPI_{VR,i}-MPI_{VR,j})<MPI_{tol}$ then
12: $SUM=SUM+MPI_{VR,j}$
13: else
14: for $k=i$ to $j-1$
15: $MPI_{ave,k}=SUM/(j-i)$
16: end for
17: Break
18: end if
19: end for
20: $i=j+1$
21: end for

B. SPR and Power Simulation

The VR-based SPR is the first stage of interaction between the VR and the physical PVS entity in Algorithm 1. Based on N_{MPI} obtained in Section II-A, the list of initial

sampling points $V=\{v_1^0, v_2^0, \ldots, v_{N_{Irr}}^0\}$ for SPR can be determined. Each sampling point in the list V is defined by:

$$v_i^0 = \left(\sum_{n=1}^{i-1} N_{MPI,n} + bN_{MPI,i} \right) \frac{V_{ocs}}{N_s} \tag{1}$$

where V_{ocs} is the open-circuit voltage of PVS; N_s is the number of series-connected PVMs in the PVS; the superscript 0 denotes the initial iteration; $i \in [1, N_{Irr}]$; and b is a constant value and can be chosen as 0.5.

b is utilized to guarantee that the sampling point falls at the midpoint of the designated I-V stair. For instance, considering the scenario depicted in Fig. 1(c), V is calculated as $\{1.0, 2.5, 4.0, 5.5\} V_{ocs}/N_s$. According to the measured current list $I=\{i_1^0, i_2^0, \ldots, i_{N_{Irr}}^0\}$, the corresponding solar irradiance level can be calculated according to (2).

$$I_{rr,i} = \frac{I_{rr,STC}(i_i^0 / I_{sc,STC})}{1+(T-T_{tc})\alpha_{tc} I_{tc}} \tag{2}$$

where $I_{rr,i}$ is the solar irradiance level of the i^{th} PVM; $I_{rr,STC}$ is the solar irradiance under the standard test the condition; $I_{sc,STC}$ is the short-circuit current of the PVM under the standard test condition; T is the ambient temperature; I_{tc} is the temperature coefficient of short-circuit current; T_{tc} is the temperature under the standard test condition; and α_{tc} is a constant and serves the purpose of converting temperature coefficients I_{tc} from percentages to Celsius.

The simulated characteristics of PVS in the VR environment can be computed using $\hat{I} = \hat{I}_{ph} - \hat{I}_D$, where $\hat{I}$ is the simulated output current; $\hat{I}_{ph}$ is the simulated light-generated current of the specified PVM; and $\hat{I}_D$ is the simulated current loss due to recombination. As the proposed formulation of the VR-simulated P-V curve neglects the impact of parallel and series resistors inherent in actual PV systems, it incorporates a power deviation mechanism. Drawing upon the analytical modelling analysis by [23], the output characteristics of PVS can be regarded as an amalgamation of the output traits of PVMs. Each MPP along the VR simulated P-V curve is bounded to exhibit a power deviation to its measured value. Furthermore, these MPPs are denoted as the simulated maximum power value $P_{VR}=\{P_{VR,1}, P_{VR,2}, \ldots, P_{VR,N_{Irr}}\}$ for a PVS with N_{Irr} different solar irradiance levels, where $P_{VR,i}$ is the VR simulated power value resulting from the previously described VR simulated P-V curve for the i^{th} search region.

C. IGMPPT

The proposed IGMPPT is conducted after SPR and power simulation. According to the VR simulated P-V curve obtained from Section II-A, the starting points for the interactive search regions are obtained. The starting point for the i^{th} search region v_i^0 is given by:

$$v_i^0 = 0.8 \sum_{n=1}^{i} N_{MPI,n} \frac{V_{ocs}}{N_s} \tag{3}$$

The selection of the constant 0.8 is derived from the established $0.8V_{OC}$-model, deliberately chosen to secure finely tuned starting points [9].

The proposed IGMPPT is conducted following a Q-learning strategy. In the i^{th} search region, the Q-learning strategy is employed to interactively determine the search step. Q-learning is a form of reinforcement learning strategy designed to maximize the rewards within an uncertain environment. The Q-learning strategy operates by responding to a state in S with an action from A, thereby guiding the selection of actions to maximize the reward r. This process is characterized as a Markov decision process. For the proposed IGMPPT, the definition and action of Q-learning are described as follows.

1) State: the state of voltage set-point at step k v_i^k is defined by $s^k \in S = \{s_0, s_1, s_2, s_3\}$, as shown in (4).

$$s^k = \begin{cases} s_0 & \Delta p_i^k > 0, \Delta v_i^k > 0 \\ s_1 & \Delta p_i^k > 0, \Delta v_i^k < 0 \\ s_2 & \Delta p_i^k < 0, \Delta v_i^k > 0 \\ s_3 & \Delta p_i^k < 0, \Delta v_i^k < 0 \end{cases} \tag{4}$$

where $\Delta p_i^k = p_i^k - p_i^{k-1}$, p_i^k is the measured power at step k; and $\Delta v_i^k = v_i^k - v_i^{k-1}$. The IGMPPT search is adjusted by the voltage step V_{step} through a Q-learning strategy. Physically, the four states s_0-s_4 describe the approximate distance and direction of the agent from the MPPs.

2) Action: the set of possible actions, denoted as A, consists of desired voltage perturbations. The selection and setting of the step size depend on the performance of the DC-DC controller and the desired control precision of the PV system. The flexible action set $A=\{\Delta v_0, \Delta v_1, \ldots, \Delta v_{N_A}\}$, by allowing variable-step tracking, enables the proposed IGMPPT to adapt more precisely to different conditions.

3) Reward: the reward function r is defined as:

$$r = \frac{p_i^k}{P_{stc}} \tag{5}$$

where P_{stc} is the power output under the standard test condition.

4) Policy: the Q value update function for the transition from state s^k to s^{k+1} with action a is outlined as:

$$\mathcal{V}(s^{k+1}) = r(s, a, s^{k+1}) + \gamma \mathcal{V}(s^k) \tag{6}$$

where $r(s, a, s^{k+1})$ is the reward obtained after taking an action a; $\mathcal{V}(\cdot)$ is the value function that uses expectations to make predictions about future rewards; and γ is the discount rate. The action for search region at state s^k is determined according to (7).

$$V_{step}(s^{k+1}) = \max_{a \in A} \mathcal{V}(s^{k+1}) \tag{7}$$

In the proposed IGMPPT, the voltage step V_{step} in a specified search region aligns with the action associated with the highest value function. During the IGMPPT process, the algorithm interactively compares the measured power of each search region with the VR simulated power at each iteration of other search regions. If the VR simulated power in the current search region is less than the measured power of any other search region, the current search region will be discarded, because there is already at least one search region with measured power higher than its possible maximum power. Intuitively, the update strategy in each search region is described as:

$$\forall j: p_j^{\max} \le P_{VR,i} \rightarrow v_i^{k+1} = v_i^k + V_{step}(v_i^k) \tag{8}$$

where $p_j^{\max}$ is the maximum power value of the j^{th} search region during the tracking process, and $j \in [1, N_{Irr}]$.

A demonstration of the proposed IGMPPT is shown in Fig. 2. In Fig. 2(a), the left-side search region (search region 1) is discarded because its VR simulated power $P_{VR,1}$ is lower than the measured power in search region 2 p_2^1. In Fig. 2(b), the search continues in both search regions because they satisfy (8). A Q-learning strategy is applied to refine the search for GMPP. This iterative process continues until only one remaining search region attains a measured power higher than all the simulated power values of other regions.

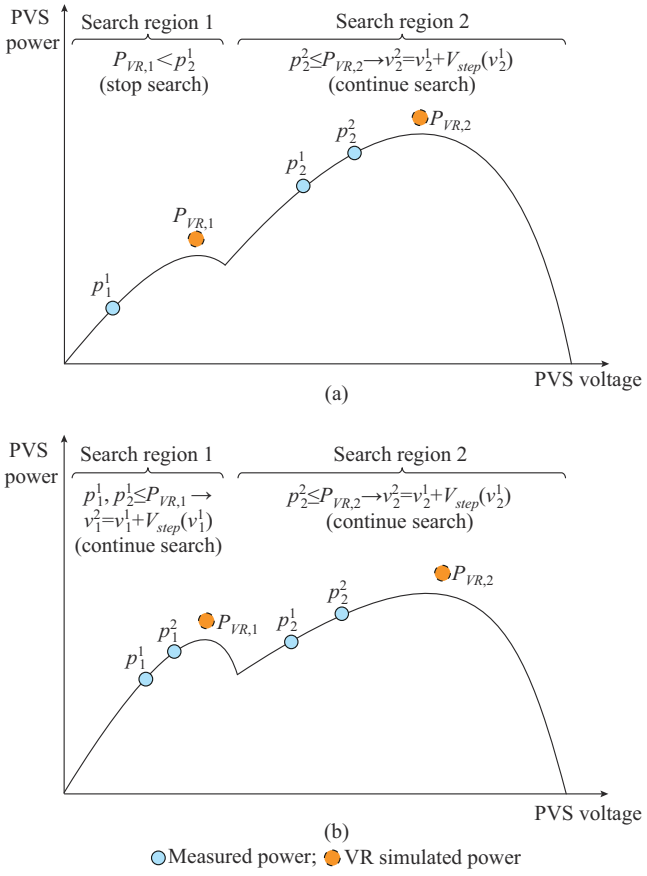

Fig. 2. Demonstration of proposed IGMPPT. (a) Stop search in region 1 but continue search in region 2. (b) Continue search in both regions 1 and 2.

As shown in Fig. 3, the function *len*(·) is employed to assess the number of effective search regions. This paper can be divided into two distinct phases. The initial phase encompasses SPR and power simulation, while the subsequent phase involves online tracking. Different from the conventional GMPPT methods, the proposed IGMPPT interactively depicts the geographic, spatio, and temporal characteristics of the PV system. This foundational understanding facilitates SPR and power simulation. Utilizing this information, the subsequent tracking process with interactive search takes place. Through the interaction of data from the VR environment, the exploration area of the search region is gradually refined. This refinement continues until the final search region, where the GMPP is located, is determined.

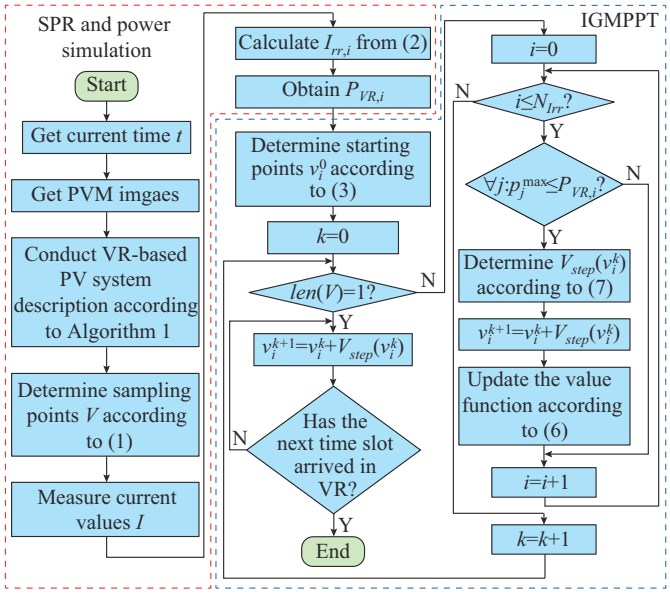

Fig. 3. Flowchart for this paper.

III. Experimental Results and Discussion

The proposed IGMPPT is designed for real-world PV entity manipulation using information sourced from the VR. The performance of the proposed IGMPPT is assessed from two phases. In the first phase, the evaluations include SPR and power simulation assessments, aimed at evaluating its capabilities in depicting the spatio and temporal characteristics of the PV systems. The second phase entails evaluating the tracking efficiency and accuracy. The experimental setup, as illustrated in Fig. 4, is established to assess the performance of the proposed IGMPPT. For the purpose of experimentally validating the proposed IGMPPT, Unity scripts are executed on the computer. The boost converter is controlled by an STM32 micro-controller. Regarding VR runtime, it is dependent on the computational capabilities of the system. We use a computer equipped with an Intel Core i7-10750H CPU and an Intel UHD Graphics GPU to simulate shading scenarios over a day. The image size is 580×580 pixels, and the simulation covers the time period from 05:30 to 19:00. Across different time resolutions, i.e., 1 min, 5 min, and 10 min, the runtime on the computer is 35 s, 8 s, and 5 s, respectively.

A. SPR and Power Simulation Evaluations

The output characteristics of the PV system shown in Fig. 4(a) are recorded by a PROVA-1011 solar system analyzer on three different days: a cloudy day (Day-1), a windy day (Day-2), and a sunny day (Day-3). The solar irradiance simulation resolution for the VR section is set to be 1 W/m^2. The error between the VR simulated power and the measured power of the proposed IGMPPT is depicted in Fig. 5. The mean errors recorded are 0.1608 W, 0.2281 W, and 0.4844 W on Day-1, Day-2, and Day-3, respectively. Furthermore, a simulated power deviation of around 5% is detected. It is worth highlighting that this power bias becomes more pronounced at elevated power levels, especially during midday on sunny days. This phenomenon primarily stems from the increased power output of PV system when exposed to ample solar irradiance conditions.

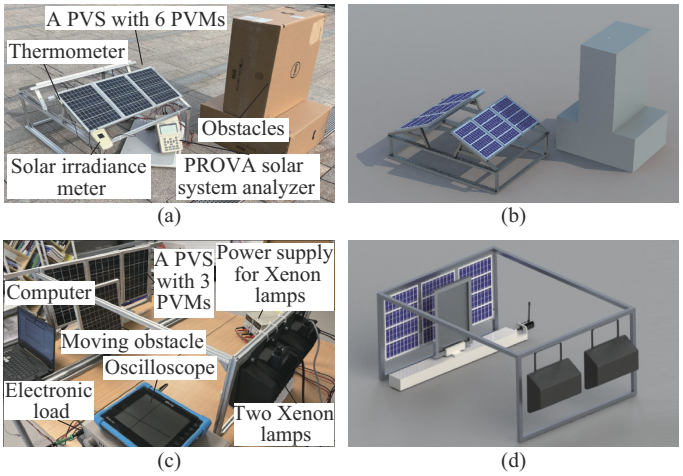

Fig. 4. Test platforms and experimental arrangement. (a) Experimental setup for SPR and power simulation test. (b) VR setup for SPR and power simulation test. (c) Experimental setup for GMPPT test. (d) VR setup for GMPPT test.

For the test results of Day-1, Day-2, and Day-3, we plot Fig. 6 with temperature on the *x*-axis and solar irradiance on the *y*-axis. We employ colour depth to represent the magnitude of absolute estimation errors. The average absolute estimation errors on Day-1, Day-2, and Day-3 are 0.2319 W, 0.2687 W, and 0.5220 W, respectively. Due to the high modelling accuracy of the PV system, temperature does not significantly affect the power error. As a result, the system modelling error values remain consistently within a fixed range across the tested temperature range.

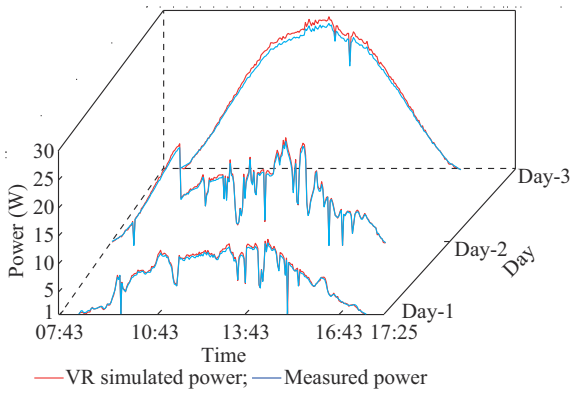

Fig. 5. Error between VR simulated power and measured power of proposed IGMPPT on Day-1, Day-2, and Day-3.

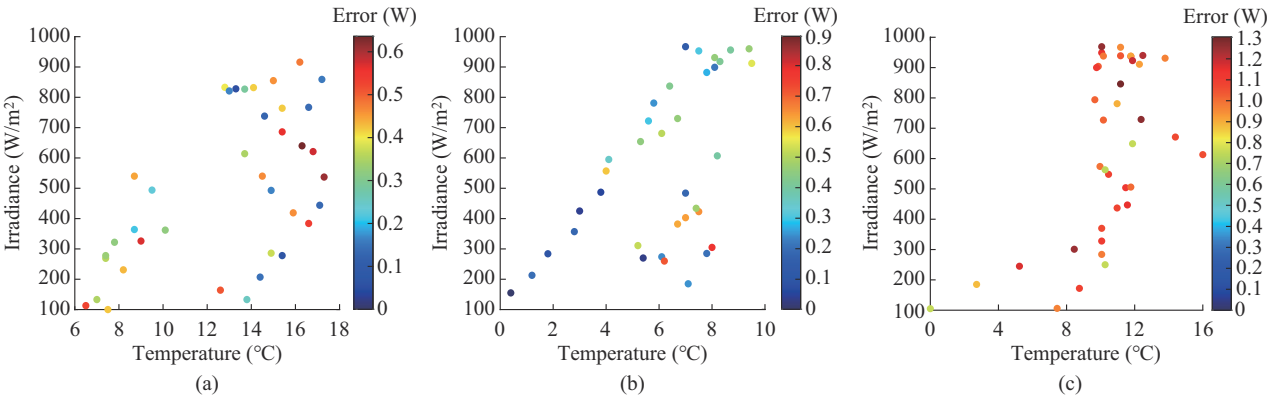

Fig. 6. Temperature, solar irradiance, and absolute estimation error on Day-1, Day-2, and Day-3. (a) Day-1. (b) Day-2. (c) Day-3.

A comparative evaluation of the proposed IGMPPT against P&O [4], LPSO [5], and RL-Beta [17] is conducted for a PV system equipped with six Jianghai 10 W (JH-10) PVMs, as shown in Fig. 4(a). The six PVMs are arranged in such a way that three PVMs are positioned on each of the two 30° slopes. This configuration results in the creation of a double-slope building structure. To replicate building shapes, a construction involving two cardboard boxes is employed to create an irregular adjacent building structure. Its corresponding VR setup is shown in Fig. 4(b). In the P&O, a voltage step of 2.5 V is employed. For the LPSO, the particle count is set to be 3, and the activation threshold is set to be 5%, as suggested in [5]. In the RL-Beta, the same learning rules from the original papers are employed to formulate action strategies. SC-1, SC-2, and SC-3 represent three distinct PSCs obtained from on-site data collection using the PROVA-1011 solar system analyzer. Table I provides the irradiance of each PVM, temperature, and the expected PVS voltage and power of GMPP (V_{GMPP} and P_{GMPP}) under SC-1, SC-2, and SC-3.

TABLE I
IRRADIANCE OF EACH PVM, TEMPERATURE, AND EXPECTED PVS VOLTAGE AND POWER OF GMPP UNDER SC-1, SC-2, AND SC-3

PSC	Irradiance of each PVM (W/m^2)						Temperature (°C)	V_{GMPP} (V)	P_{GMPP} (W)
	PVM1	PVM2	PVM3	PVM4	PVM5	PVM6			
SC-1	460	460	460	130	130	130	8.5	25.6	10.5
SC-2	330	330	110	110	110	110	5.3	53.5	6.4
SC-3	450	450	330	110	110	110	3.2	23.5	12.4

The tracking performances of different methods under three PSCs, depicting the transitions from SC-1 to SC-2 and from SC-2 to SC-3, are illustrated in Fig. 7. As shown in Fig. 8, under the SC-1, V_{GMPP} is 25.5 V and P_{GMPP} is 10.5 W. Under SC-2, V_{GMPP} is 53.5 V and P_{GMPP} is 6.4 W. Under SC-3, V_{GMPP} is 23.5 V and P_{GMPP} is 12.4 W.

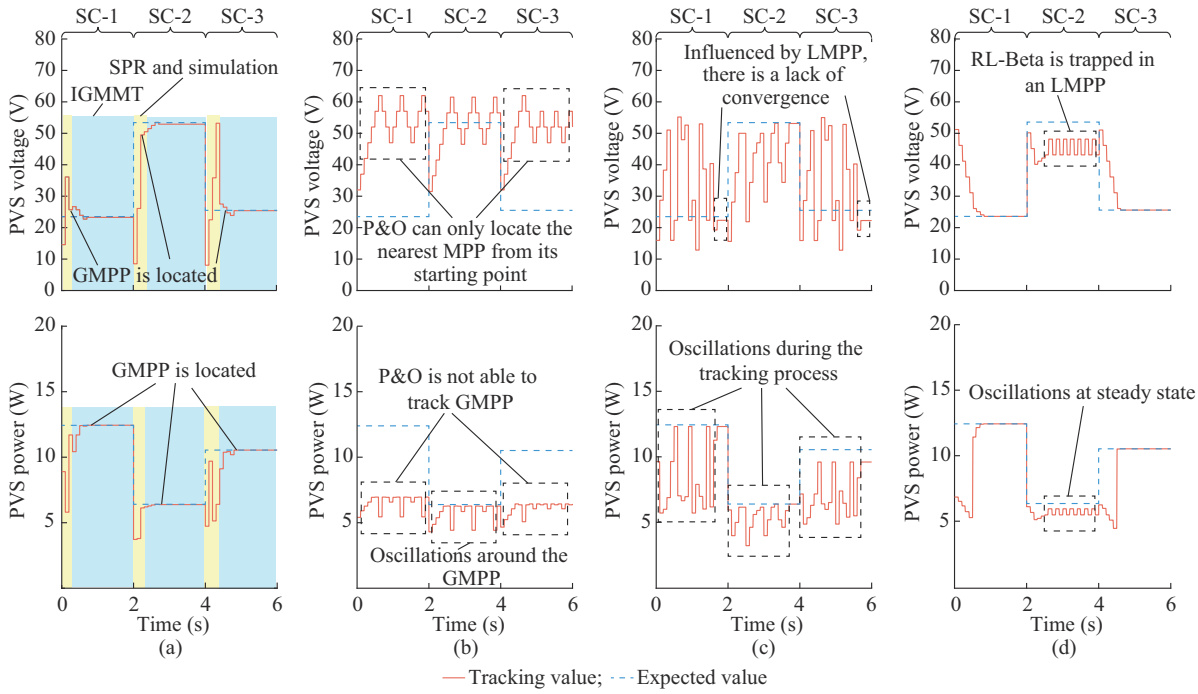

Fig. 7. Tracking performance of different methods under three PSCs. (a) Proposed IGMPPT. (b) P&O. (c) LPSO. (d) RL-Beta.

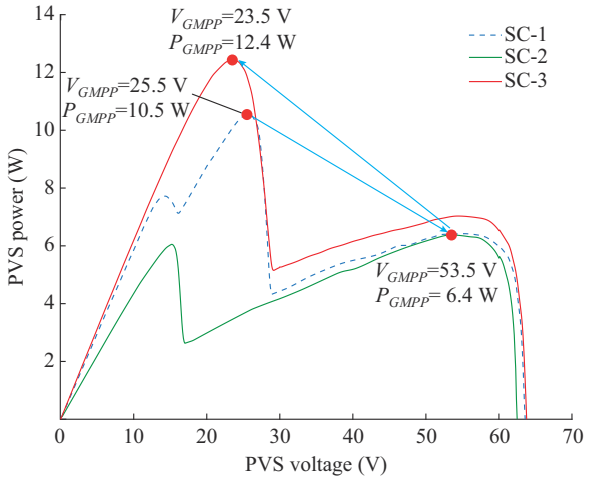

Fig. 8. *P-V* curves under SC-1, SC-2, and SC-3.

B. GMPPT Evaluations

Under SC-1, the sampling voltage list V is {14.6, 36.1}V, and the corresponding current list I is {0.61, 0.16}A. After the SPR and power simulation, P_{VR} is {13.6, 8.7}W. The measured power in the first iteration p_1^1 is 10.4 W, which exceeds the simulated power value $P_{VR,2}$ of 8.7 W. Therefore, the voltage range $[0, V_{ocm}]$, where V_{ocm} represents the open-circuit voltage of the PVM, becomes the sole surviving search region in the first iteration, and the search continues until the GMPP is determined. Under SC-1, the P&O is unsuccessful in accurately locating the GMPP and becomes stuck in the local maximum power point (LMPP). Although the LPSO is capable of tracing the GMPP, it exhibits greater oscillations than the proposed IGMPPT, leading to a decreased efficiency of 23%. Although the RL-Beta manages to track the GMPP, it incurs a time cost twice as much as that of the proposed IGMPPT.

Under SC-2, the sampling voltage list V is {8.5, 26.1}V, and the corresponding current list I is {0.44, 0.15}A. After SPR and power simulation, P_{VR} is {5.8, 6.5}W. The measured power in the first iteration p_2^1 is 6.1 W, surpassing the simulated power value $P_{VR,1}$ of 5.8 W. The voltage range $[V_{ocm}, 2V_{ocm}]$ becomes the sole surviving search region after the first iteration. Under SC-2, the LPSO faces challenges in accurately monitoring the GMPP and introduces elevated oscillations, making it difficult to mitigate the impact of the LMPP located within the voltage range $[0, V_{ocm}]$ during subsequent tracking attempts. The RL-Beta successfully identifies the GMPP but with a deviation of 3.4 V. This discrepancy under complex PSCs can be attributed to the reliance of RL-Beta on the pre-trained model.

Under SC-3, the sampling voltage list V is {8.5, 22.1, 35.8}V, and the corresponding current list I is {0.59, 0.43, 0.14}A. After SPR and power simulation, P_{VR} is {8.2, 10.9, 7.2}W. In the first iteration, p_1^1 is discarded because $P_{VR,1}$ is less than either p_2^1 or p_3^1. In the second iteration, the search region $[2V_{ocm}, 3V_{ocm}]$ is discarded because $P_{VR,3}$ of 7.2 W is less than p_2^2 of 9.2 W. After that, the search region $[V_{ocm}, 2V_{ocm}]$ becomes the last search region. The search continues in the last search region to identify the GMPP. The P&O fails under SC-3 because its starting point is far from the

GMPP. Since the MPPs located in $[0, V_{ocm}]$ and $[2V_{ocm}, 3V_{ocm}]$ have similar maximum power values under SC-3, the LPSO and RL-Beta produce larger oscillations than the proposed IGMPPT and cause around 20% and 22% efficiency losses, respectively.

The results of the proposed GMPPT are quantitatively compared with P&O, LPSO, and RL-Beta. The tracking accuracy of GMPP power P_{acc}, the tracking efficiency of GMPP power P_{eff}, the tracking error of GMPP voltage V_{err}, and the root mean square value of GMPP power P_{rms} during the tracking process are used to evaluate the tracking performance, as summarized in Table II.

TABLE II
COMPARISONS AMONG PROPOSED IGMPPT, P&O, LPSO, AND RL-BETA UNDER SC-1, SC-2, AND SC-3

PSC	P_{eff} (%)				P_{acc} (%)				V_{err} (V)				P_{rms} (W)			
	Proposed IGMPPT	P&O	LPSO	RL-Beta	Proposed IGMPPT	P&O	LPSO	RL-Beta	Proposed IGMPPT	P&O	LPSO	RL-Beta	Proposed IGMPPT	P&O	LPSO	RL-Beta
SC-1	94.30	52.49	71.25	86.73	99.91	56.12	98.98	98.52	0.16	33.50	1.17	0.17	1.75	5.93	4.47	3.17
SC-2	94.00	89.54	82.20	89.25	99.30	98.25	99.20	96.27	0.80	3.10	0.16	3.40	0.84	1.00	1.40	0.74
SC-3	90.87	57.89	69.03	87.91	99.84	61.21	91.08	99.47	0.24	26.50	3.24	0.47	2.03	4.46	3.69	2.55

It can be observed that the proposed IGMPPT achieves the highest average P_{eff} of 93.06% and average P_{acc} of 99.68% compared with the P&O, LPSO, and RL-Beta. Under all PSCs, the P&O can only track the LMPP closest to its starting point, which results in a power loss of over 5 W under SC-1 and SC-3. Besides, the proposed IGMPPT achieves the lowest P_{rms} during the tracking process under SC-1, SC-2, and SC-3. The LPSO can successfully track the GMPP, but it requires collecting more data points, leading to inefficient operations. In the worst case, P_{eff} of LPSO is only 69.03%. The perturbation of LPSO is significantly larger than that of the proposed IGMPPT. The performance of RL-Beta is second only to the proposed IGMPPT. There is still a gap in the tracking efficiency. In terms of tracking efficiency, the proposed IGMPPT achieves an average improvement of nearly 5% over RL-Beta. In conclusion, the proposed IGMPPT obtains the best performance in terms of P_{eff} and P_{acc}. Even under SC-2, where two MPPs with a similar values of peaks exist, the proposed IGMPPT can successfully discriminate and track the true GMPP. In contrast, the LPSO fails to track GMPP due to the random factors that affect the convergence processes of their search regions, leading to premature convergence and potentially missing the true GMPP values. The reason is that the VR modelling enables to obtain an accurate sampling point list in the VR environment. After completing the SPR and power simulation, the error of VR in the real world is further corrected. With more measured data during the tracking process, each search region is given a clear indication of their potential maximum power value and a rigorous abandonment mechanism, enabling the proposed IGMPPT to perform an efficient search.

An experimental setup, as depicted in Fig. 4(c), is employed to validate the performance of the proposed IGMPPT. Its corresponding VR setup is shown in Fig. 4(d). The experimental setup includes 3 JH-10 PVMs to form the PV system, a moving baffle to simulate shadows, two 500 W Xenon lamps to simulate solar light, and a programmed electronic load directly connected to the output of PVS. The performances of the proposed IGMPPT, P&O, LPSO, and RL-Beta are evaluated under three different PSCs: SC-4, SC-5, and SC-6. Table III provides the irradiance of each PVM, temperature, and expected PVS voltage and power of the GMPPs for the PVS under SC-4, SC-5, and SC-6.

TABLE III
IRRADIANCE OF EACH PVM, TEMPERATURE, AND EXPECTED PVS VOLTAGE AND POWER OF GMPPS UNDER SC-4, SC-5, AND SC-6

PSC	Irradiance (W/m^2)			Temperature (°C)	V_{GMPP} (V)	P_{GMPP} (W)
	PVM1	PVM2	PVM3			
SC-4	690	690	690	24.3	42.0	29.0
SC-5	650	650	170	26.1	27.6	18.2
SC-6	720	234	234	27.5	46.8	11.8

As demonstrated in Fig. 9(a), (e), (i), the VR offers sampling points for SPR and power simulation. Among the different PSCs, SC-4 only requires one sampling point due to the UIC.

Moreover, SC-5 and SC-6 necessitate two sampling points to capture the shading patterns. The number of sampling points is dependent on the number of irradiance levels for the PVS. The proposed IGMPPT shows faster tracking speed and higher tracking efficiency compared with others. During the experimental assessment, the entire process of confirming the GMPP takes approximately 2.0 s for SC-4, 2.5 s for SC-5, and 2.5 s for SC-6, respectively. In contrast to the P&O, LPSO, and RL-Beta, the proposed IGMPPT shows enhanced efficiency. This advantage can be traced back to its adaptive strategy, where the number of search regions in the proposed IGMPPT depends on the shading conditions of the system. Furthermore, the search regions are strategically decreased when their potential to yield improved performance is deemed unlikely. Besides, the P&O, LPSO, and RL-Beta follow fixed search patterns and are more reliant on the starting points, which results in a decrease in tracking accuracy. As shown in Fig. 9(b), (f), (j), the P&O can only track to the nearest MPP from its starting point. The RL-Beta, as shown in Fig. 9(d), (h), and (l), stops near the GMPP, with accuracy dependent on the minimum step size. This is because the RL-Beta is only available for UICs. In contrast, the proposed IGMPPT overcomes the aforementioned limitations and successfully tracks the GMPP under all PSCs. The GMPP power values achieved in the experiments are 14.5 W

for SC-4, 9.1 W for SC-5, and 5.9 W for SC-6. These results validate the superiority of the proposed IGMPPT in achieving accurate and efficient tracking of the GMPP in PV systems.

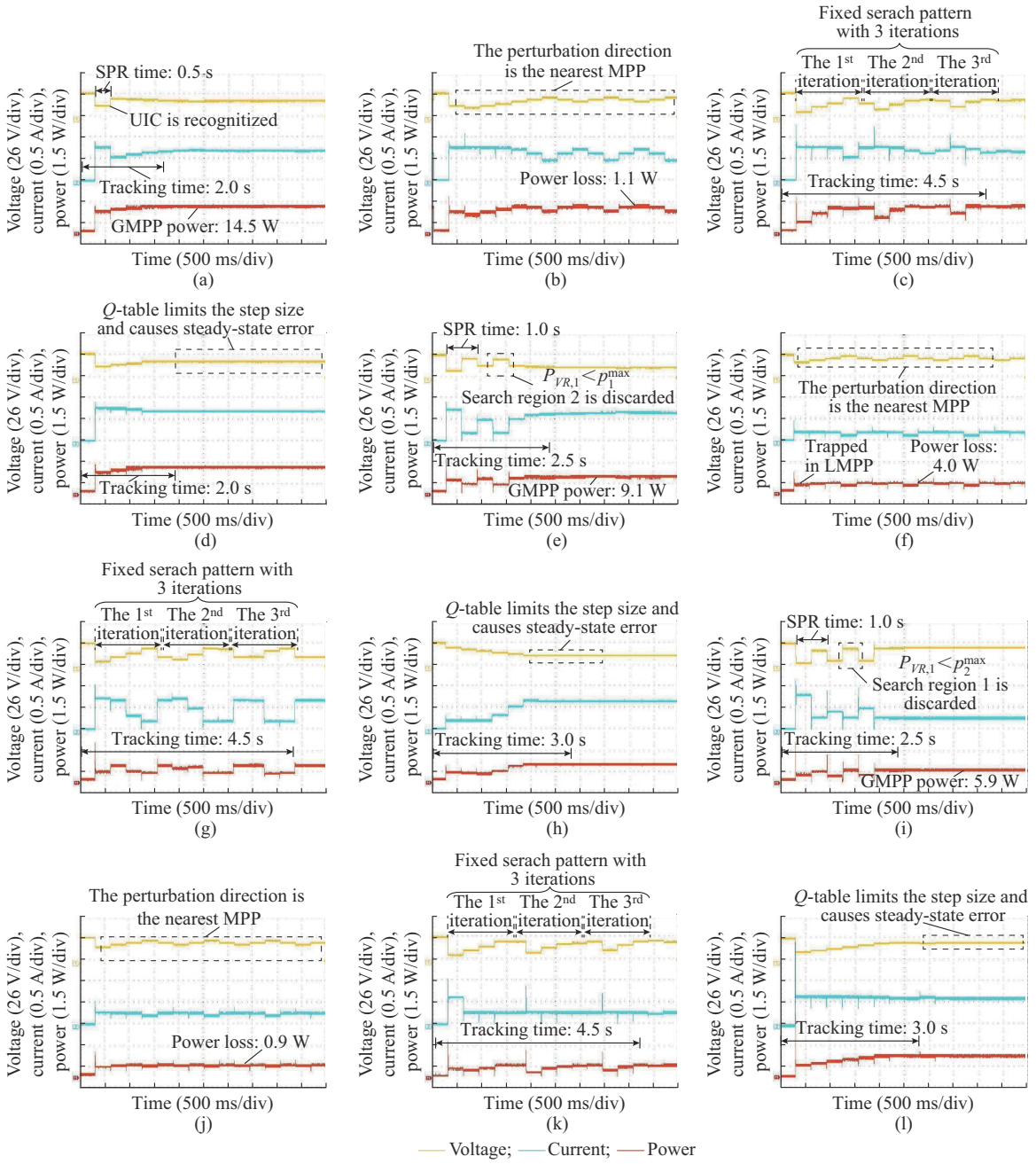

Fig. 9. Tracking performance of different methods under SC-4, SC-5, and SC-6 captured by oscilloscope. (a) Proposed IGMPPT under SC-4. (b) P&O under SC-4. (c) LPSO under SC-4. (d) RL-Beta under SC-4. (e) Proposed IGMPPT under SC-5. (f) P&O under SC-5. (g) LPSO under SC-5. (h) RL-Beta under SC-5. (i) Proposed IGMPPT under SC-6. (j) P&O under SC-6. (k) LPSO under SC-6. (l) RL-Beta under SC-6.

IV. Conclusion

This paper introduces a novel VR-based IGMPPT method for accurate and efficient GMPPT in PV systems. The proposed IGMPPT leverages VR technology to simulate the spatial and temporal characteristics of a PV system, making it effective in the SPR and determination of search regions through iterative searches. Experimental results demonstrate that the proposed IGMPPT attains an efficiency rate surpassing 90%, accompanied by an accuracy level exceeding 99% in the selected test scenarios. Compared with P&O, LPSO, and RL-Beta methods, the proposed IGMPPT increases tracking efficiency by 27%, 19%, and 5%, respectively, while maintaining a promising tracking accuracy.

References

[1] G. G. Platero, M. G. Casado, M. P. García *et al.*, "CECRE: Supervision and Control of Spanish Renewable Energies in the Last 15 years," *Journal of Modern Power Systems and Clean Energy*, vol. 10, no. 2, pp. 269-276, Mar. 2022.

[2] K. Y. Yap, C. R. Sarimuthu, and J. M.-Y. Lim, "Artificial intelligence based MPPT techniques for solar power system: a review," *Journal of Modern Power Systems and Clean Energy*, vol. 8, no. 6, pp. 1043-1059, Nov. 2020.
[3] J. Dadkhah and M. Niroomand, "Optimization methods of MPPT parameters for PV systems: review, classification, and comparison," *Journal of Modern Power Systems and Clean Energy*, vol. 9, no. 2, pp. 225-236, Mar. 2021.
[4] N. Karami, N. Moubayed, and R. Outbib, "General review and classification of different MPPT Techniques," *Renewable and Sustainable Energy Reviews*, vol. 68, pp. 1-18, Feb. 2017.
[5] S. Makhloufi and S. Mekhilef, "Logarithmic PSO-based global/local maximum power point tracker for partially shaded photovoltaic systems," *IEEE Journal of Emerging and Selected Topics in Power Electronics*, vol. 10, no. 1, pp. 375-386, Feb. 2022.
[6] K. Ishaque and Z. Salam, "A deterministic PSO maximum power point tracker for PV system under PSC," *IEEE Transactions on Industrial Electronics*, vol. 60, no. 8, pp. 3195-3206, May 2012.
[7] D. F. Teshome, C. H. Lee, Y. W. Lin *et al*., "A modified firefly algorithm for photovoltaic maximum power point tracking control under partial shading," *IEEE Journal of Emerging and Selected Topics in Power Electronics*, vol. 5, no. 2, pp. 661-671, Jun. 2017.
[8] V. Jately, S. Bhattacharya, B. Azzopardi *et al*., "Voltage and current reference based MPPT under rapidly changing irradiance and load resistance," *IEEE Transactions on Energy Conversion*, vol. 36, no. 3, pp. 2297-2309, Sept. 2021.
[9] Z. Bi, J. Ma, K. L. Man *et al*., "An enhanced $0.8V_{OC}$-model-based global maximum power point tracking method for photovoltaic systems," *IEEE Transactions on Industry Applications*, vol. 56, no. 6, pp. 6825-6834, Nov. 2020.
[10] A. Gholami, M. Ameri, M. Zandi *et al*., "Step-by-step guide to model pv panels: an up-to-date comparative review study," *IEEE Journal of Photovoltaics*, vol. 12, no. 4, pp. 915-928, May 2022.
[11] S. Shukla, B. Singh, P. Shaw *et al*., "A new analytical MPPT-based induction motor drive for solar PV water pumping system with battery backup," *IEEE Transactions on Industrial Electronics*, vol. 69, no. 6, pp. 5768-5781, Jun. 2022.
[12] S. Senthilkumar, V. Mohan, S. P. Mangaiyarkarasi *et al*., "Analysis of single-diode PV model and optimized MPPT model for different environmental conditions," *International Transactions on Electrical Energy Systems*, vol. 2022, p. 4980843, Jan. 2022.
[13] V. L. Mishra, Y. K. Chauhan, and K. S. Verma, "A critical review on advanced reconfigured models and metaheuristics-based MPPT to address complex shadings of solar array," *Energy Conversion and Management*, vol. 269, p. 116099, Oct.2022.
[14] N. Swaminathan, N. Lakshminarasamma, and Y. Cao, "A fixed zone P&O MPPT technique for a standalone distributed PV system," *IEEE Journal of Emerging and Selected Topics in Power Electronics*, vol. 10, no. 1, pp. 361-374, Mar. 2022.
[15] J. S. Koh, R. H. Tan, W. H. Lim *et al*., "A modified PSO for efficient MPPT under PSC," *IEEE Transactions on Sustainable Energy*, vol. 14, no. 3, pp. 1-12, Mar. 2023.
[16] M. C. Cavalcanti, F. Bradaschia, A. J. do Nascimento *et al*., "Hybrid maximum power point tracking technique for PV modules based on a double-diode model," *IEEE Transactions on Industrial Electronics*, vol. 68, no. 9, pp. 8169-8181, Sept. 2021.
[17] D. Lin, X. Li, S. Ding *et al*., "Self-tuning MPPT scheme based on reinforcement learning and beta parameter in PV power systems," *IEEE Transactions on Power Electronics*, vol. 36, no. 12, pp. 13826-1 838, Jun. 2021.
[18] M. Dehghani, M. Taghipour, G. B. Gharehpetian *et al*., "Optimized fuzzy controller for MPPT of grid-connected PV systems in rapidly changing atmospheric conditions," *Journal of Modern Power Systems and Clean Energy*, vol. 9, no. 2, pp. 376-383, Mar. 2021.
[19] K. Danyluk, T. Ulusoy, W. Wei *et al*., "Touch and beyond: comparing physical and virtual reality visualizations," *IEEE Transactions on Visualization and Computer Graphics*, vol. 28, no. 4, pp. 1930-1940, 2022.
[20] J. M. G. Lopez, R. O. J. Betancourt, J. M. R. Arredondo *et al*., "Incorporating VR into the teaching and training of grid-tie photovoltaic power plants design," *Applied Sciences*, vol. 9, no. 21, p. 4480, Oct. 2019.
[21] B. Celik, E. Karatepe, N. Gokmen *et al*., "A VR study of surrounding obstacles on biPV systems for estimation of long-term performance of partially shaded PV arrays," *Renewable Energy*, vol. 60, pp. 402-414, Dec. 2013.
[22] J. Pinthong and W. Kaewmanee, "VR of solar farm for the solar energy system training," in *Proceedings of 2020 5th International STEM Education Conference (iSTEM-Ed)*, Hua Hin, Thailand, Nov. 2020, pp. 2-4.
[23] J. Ma, D. Hong, K. Wang *et al*., "Analytical modeling and parameter estimation of photovoltaic strings under partial shading conditions," *Solar Energy Materials and Solar Cells*, vol. 235, p. 111494, Jan. 2022.

Kangshi Wang received the M.Sc. degree in electrical engineering with excellence from the University of New South Wales, Sydney, Australia, in 2019. Currently, he is pursuing the Ph.D. degree in computer science at the University of Liverpool, Liverpool, U.K.. His research interests include intelligent optimization, machine learning, and renewable energy systems.

Jieming Ma received the M. Sc. degree in advanced microelectronic systems engineering from the University of Bristol, Bristol, U.K., in 2010, and the Ph.D. degree in computer science from the University of Liverpool, Liverpool, U.K., in 2014. From 2015 to 2017, he was a Lecturer with the Suzhou University of Science and Technology, Suzhou, China. He is currently an Associate Professor with the Xi'an Jiaotong-Liverpool University, Suzhou, China. His research interests include intelligent optimization, machine learning, and applications in renewable energy systems.

Xiao Lu is pursuing the B.Eng. degree in electronic science and technology in Xi'an Jiaotong-Liverpool University, Suzhou, China. His research interests include hardware accelerator design using field programmable gate arrays (FPGAs) to improve processing speed, cost and power, and maximizing power point tracking for photovoltaic panels.

Jingyi Wang received the B. Eng. degree in digital media technology from Xi'an Jiaotong-Liverpool University, Suzhou, China, in 2023. His research interests include digital twins, embedded system, robotics, brain-inspired intelligence, and computational social science.

Ka Lok Man received the Dr. Eng. degree in electronic engineering from the Politecnico di Torino, Turin, Italy, in 1998, and the Ph.D. degree in computer science from Technische Universiteit Eindhoven, Eindhoven, The Netherland, in 2006. He is currently a Professor in Computer Science and Software Engineering with Xi'an Jiaotong-Liverpool University, Suzhou, China. His research interests include formal methods and process algebras, embedded system design and testing, and photovoltaics.

Kaizhu Huang received the bachelor's degree from Xi'an Jiaotong University, Xi'an, China, in 1997, the master's degree from the Institute of Automation, Chinese Academy of Sciences, Beijing, China, in 2000, and the Ph.D. degree from Chinese University of Hong Kong (CUHK), Hong Kong, China, in 2004. His research interests include machine learning, neural information processing, and pattern recognition.

Xiaowei Huang is the Professor of Computer Science at the University of Liverpool, Liverpool, U.K., and serves as the Head of the Trustworthy Autonomous Cyber Physical System Lab. His research interests include machine learning, formal methods, robotics, trustworthy artificial intelligence (AI), verification, explainable AI, and AI safety and security.